Lamina Cribrosa Imaging

Tae-Woo Kim and Eun Ji Lee

Abstract

Glaucoma is characterized by the loss of retinal ganglion cells and axons. Although the pathogenesis of glaucomatous optic neuropathy is not fully elucidated, it is generally considered that axonal damage is the earliest event in the process of cell death. Since lamina cribrosa (LC) is the putative site of axonal injury, understanding the changes in the LC and its effect on the axons are essential to understand the pathophysiology of glaucomatous optic neuropathy.

With the emergence of spectral domain optical coherence tomography (SD-OCT), it became feasible to image the LC in patients. Using this noninvasive technique, various observations have been reported including dynamic features along the course of disease and according to the variation of intraocular pressure. These data help understand the optic nerve head biomechanics in the development and progression of glaucoma. Although the image quality of LC obtained by OCT is not fully satisfactory, postprocessing technique is available to better visualize the LC. Yet, LC imaging is not widely used in the clinical practice. As research continues, it is expected that LC imaging will soon be implemented in the glaucoma diagnosis and patient management.

Keywords

Lamina cribrosa · Glaucoma · Lamina cribrosa curvature index · Focal lamina cribrosa defect

1 Histology of Lamina Cribrosa

Lamina cribrosa (LC) is the sieve-like connective tissue sheets which contains about 500–600 perforations (Ogden et al. 1988). The optic nerve axon bundles pass through the pores within the LC. The LC pores in the superior and inferior part are larger than those in the nasal and temporal quadrants (Morrison et al. 1989; Quigley and Addicks 1981; Radius and Gonzales 1981).

The lamina beams are composed of elastin, collagen (types I, III, IV, V and VI), laminin, and fibronectin (Goldbaum et al. 1989; Hernandez et al. 1986). The elastin is responsible for elastic property of elastic tissue (Mecham 1991). In young adults, elastin fibers are thin, long, and run longitudinally in the lamina beams (Hernandez et al. 1986). With aging, the density of elastin in the lamina increases and the elastin fibers thicken markedly to form long, tubular structures

T.-W. Kim (✉) · E. J. Lee
Seoul National University College of Medicine,
Seoul National University Bundang Hospital,
Seongnam, Korea
e-mail: twkim7@snu.ac.kr

K. H. Park, T.-W. Kim (eds.), *OCT Imaging in Glaucoma*,
https://doi.org/10.1007/978-981-16-1178-0_5

(Hernandez et al. 1989). The change in the elastin with aging probably changes the degree of elastic property of the lamina.

The beams are dense in the mid horizontal area of the optic nerve head and elevated compared to superior and inferior region, forming a bowtie-shaped ridge (Park et al. 2012a). In glaucomatous eyes, the laminar sheets are compressed and gross configuration shows backward bowing at late stage (Quigley et al. 1983).

2 LC Imaging Using OCT

LC can be visualized using spectral domain (SD)-OCT or swept source (SS)-OCT. The LC appears as a highly reflective plate in OCT images (Fig. 1). On enface OCT images, lamina pores are visible. Since the LC is located in the deep optic nerve head, LC imaging has lower signal-to-noise ratio than surface structure imaging such as retinal nerve fiber layer. To alleviate this prob-

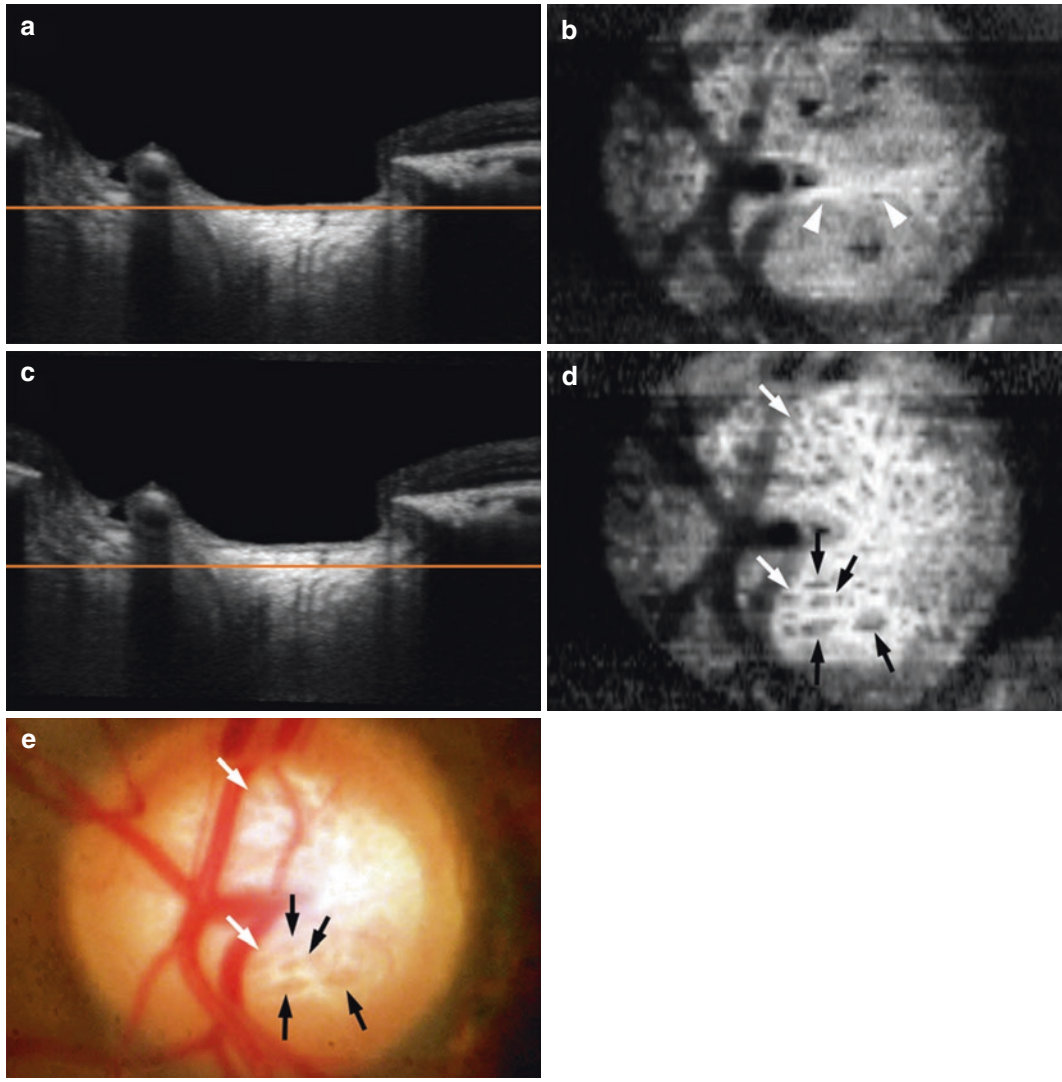

Fig. 1 Lamina cribrosa (LC) image obtained by spectral domain OCT (Spectralis, Heidelberg). B-scan (**a**, **c**) and enface (**b**, **d**) images at prelaminar (**a**, **b**) and LC (**c**, **d**) in a glaucomatous eye. The low reflective dots in the enface image through the LC consist of multiple pores that correspond to the laminar pores in the fundus photography (**e**, black arrows). Owing to the curved nature of the lamina, the enface image through the prelaminar tissue contains some lamina tissue in the central area (arrowheads). Adopted and modified from Lee et al. (2011)

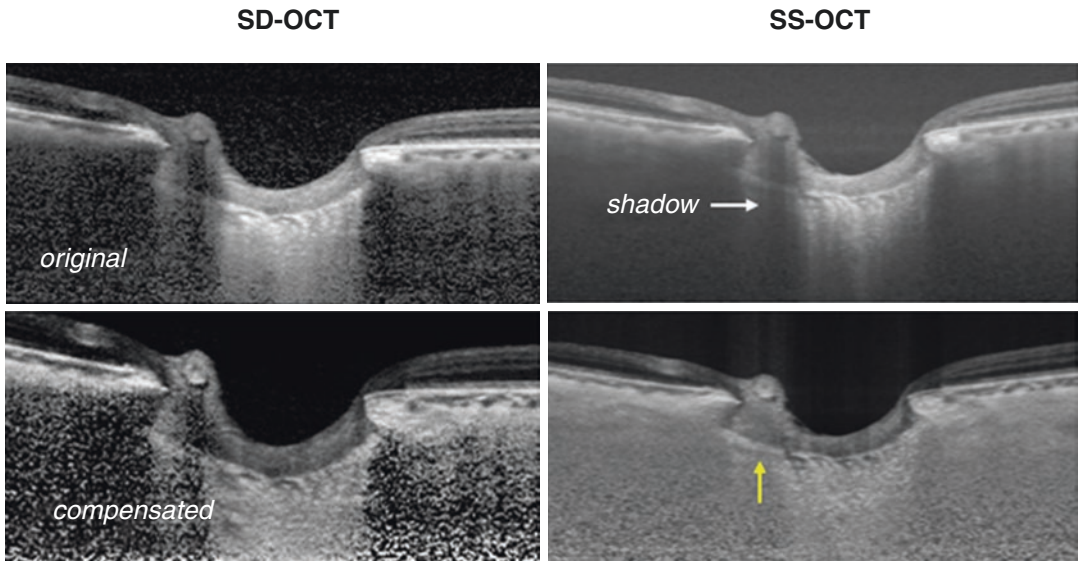

Fig. 2 Lamina cribrosa (LC) images obtained from SD-OCT (Spectralis, Heidelberg) and SS-OCT (Triton, Topcon). Images postprocessed by adaptive compensation are shown in the bottom. The LC surface is more clearly visible after adaptive compensation especially in the region of vascular shadow (yellow arrow)

lem, multiple separate scans are obtained at each scan position with the aid of eye tracking system and the result is averaged. The larger the image frames averaged, the higher the image quality. However, it requires longer time to obtain greater number of frames, which often lead to patient's poor cooperation. About 20–42 frames are generally used for SD-OCT in LC imaging (Lee et al. 2011, 2013a).

Swept Source (SS)-OCT is a newer generation of OCT that uses a short cavity swept laser with a tunable wavelength of operation. It has a longer central wavelength (1050 nm) compared to conventional SD-OCT (840 nm), providing deeper penetration. Due to this capability, high quality images can be obtained by averaging small number of image frames than SD-OCT. This enables the LC imaging to be completed within shorter period of time using SS-OCT compared to SD-OCT.

To further improve the visualization of LC, the OCT images can be postprocessed using an adaptive compensation technique which was developed by Girard and Mari et al. In this algorithm, standard compensation operations are performed until an energy threshold is reached, at which stage the compensation process is stopped to limit noise over-amplification in the deeper portion of the OCT image. This method is robust in that it can remove the shadows of blood vessels. Using this technique, the anterior surface of the LC can be more readily delineated (Fig. 2) (Girard et al. 2015).

3 Protocols to Image the LC

LC image can be evaluated using raster scans or radial scans. Each method has advantages over the other methods. Radial scan has advantage to see the LC insertion along the meridians. However, because of the bowtie-shaped central ridge of the LC (Park et al. 2012a), LC shape typically appears as a W-shape in vertical scans, and varies largely along the meridians (Fig. 3A). This large variability along the meridian makes it difficult to assess the LC shape using a simple parameter on images obtained by radial scans. Raster scans obtain multiple horizontal scans parallel to each other. The LC has a relatively regular configuration in the horizontal plane, with a flat or U-shaped appearance with different regional

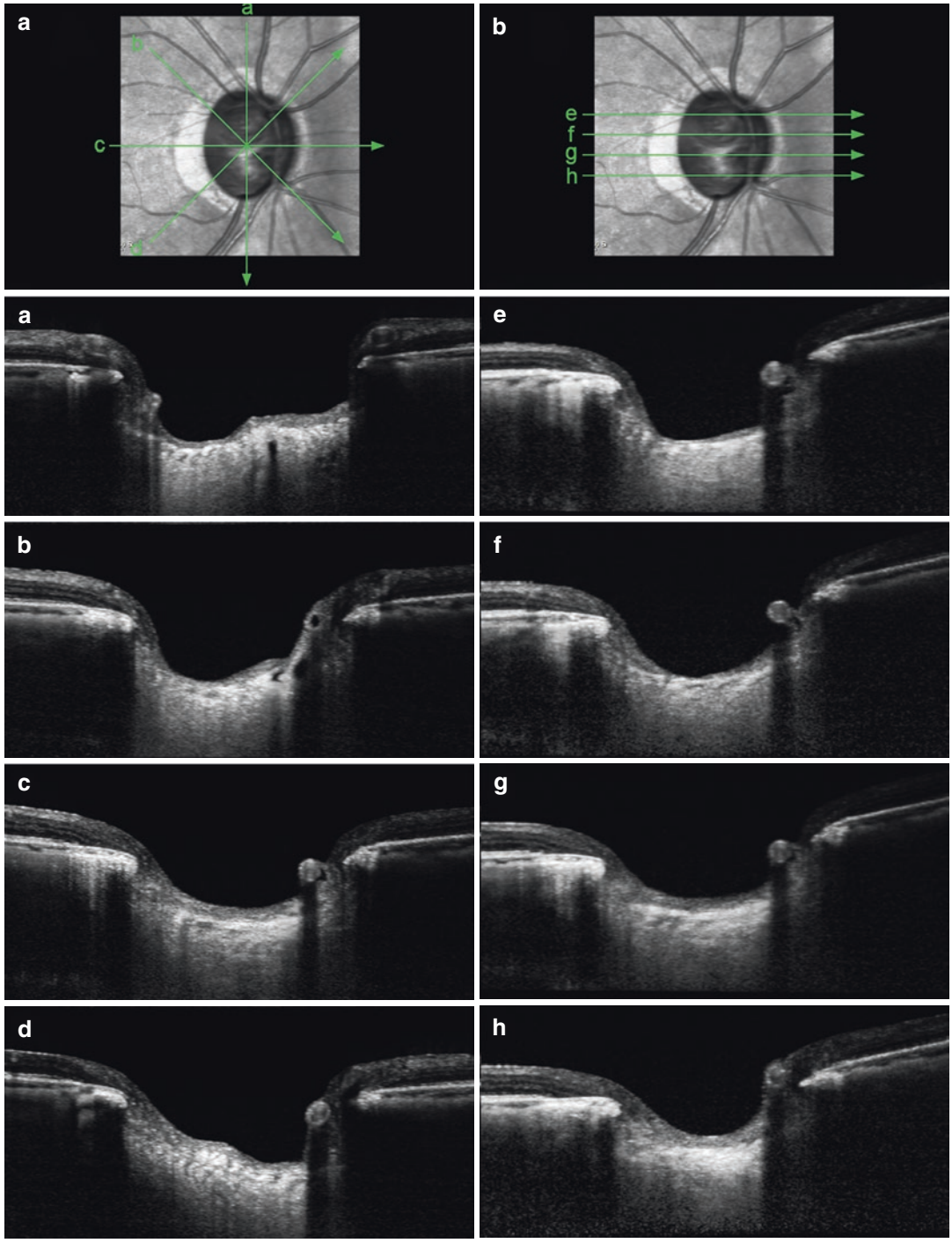

Fig. 3 Comparison of the patterns of the lamina cribrosa (LC) shape in radial (**A**), and raster (**B**) B-scans. Note that the largely different patterns of LC shape in radial scans (**A**). In contrast, the LC has a relatively regular configuration in the horizontal scans, with a flat or U-shaped appearance with different regional steepness (**B**). Note the central ridge (yellow arrow) in the vertical B-scan from 12 to 6 o/c. Adopted and modified from Lee et al. (2019)

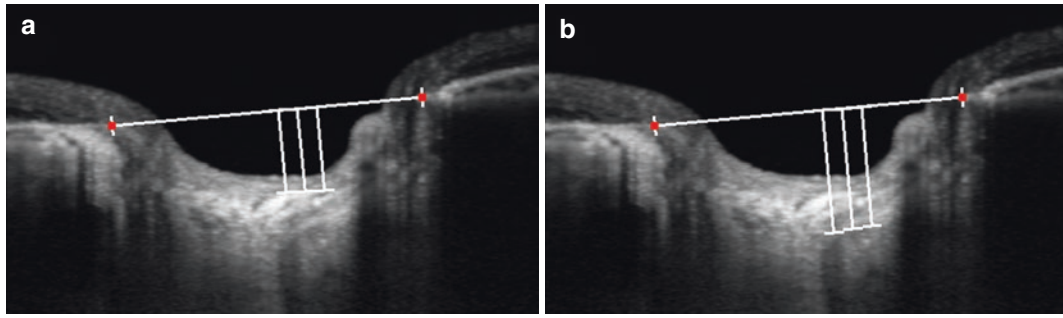

Fig. 4 Measuring the LC depth (**a**) and LC thickness. Distance to the posterior border of the LC is measured (**b**). From both measurements, the LC thickness can be calculated

steepness (Fig. 3B). Therefore, the LC shape can be readily evaluated on horizontal scans using LC curvature index (LCCI). Moreover, measuring LCCI on horizontal scans allows separate assessment of the LC morphologies in the superior and inferior region, which are often different in an individual eye (Kim et al. 2019a).

4 Indices to Evaluate LC Morphology

4.1 LC Thickness

LC thickness can be measured as the distance between the anterior and posterior LC surface (Fig. 4). Although it is measurable in many eyes, the posterior LC border is often difficult to delineate hampering the measurement of LC thickness. The LC thickness is relevant with glaucoma pathophysiology because it is associated with translaminar pressure gradient.

The LC forms the border between the intraocular space and the retrobulbar space. In general, the intraocular pressure is higher than CSF pressure. Therefore, a pressure gradient exists across the LC. At a given pressure difference between both sides of lamina, the pressure gradient is greater when the lamina is thinner (Jonas et al. 2004). An abnormal pressure gradient influences the physiology of the optic nerve fibers, with their orthograde and retrograde axoplasmic flow (Anderson and Hendrickson 1974; Quigley and Anderson 1976). Therefore, it is possible that eyes with thinner LC are more susceptible to glaucoma.

4.2 LC Depth

LC depth from Bruch's membrane opening (BMO) has been suggested as a parameter to evaluate LC morphology. Since Bruch's membrane opening is clearly visualized in most OCT images, BMO can be used as a reliable reference (Fig. 4). However, LC depth from BMO has a limitation. LC is sustained by load-bearing connective tissues of the peripapillary sclera. Thus, it would be more reasonable to assess LC morphology (and changes with IOP) from the scleral plane or directly within the LC. When the LC depth is measured from the BMO level would inappropriately include the choroidal thickness. Since the choroidal thickness varies among individuals and with aging within an individual patient (Rhodes et al. 2015), LC depth measurement form BMO may provide a biased assessment. To overcome this limitation, Vianna et al. (2017) suggested anterior scleral opening as a more reliable reference structure to measure the LC position. The measured depth is not influenced by the choroidal thickness. However, the anterior scleral opening is often difficult to reliable detect in OCT images.

4.3 LC Curvature Index (LCCI)

Since LC deformation occurs as a posterior bowing pattern, measuring the LC curve can be used to evaluate the LC strain. Differing methods have been suggested to evaluate the LC curve. Lee et al. suggested a simple parameter which was

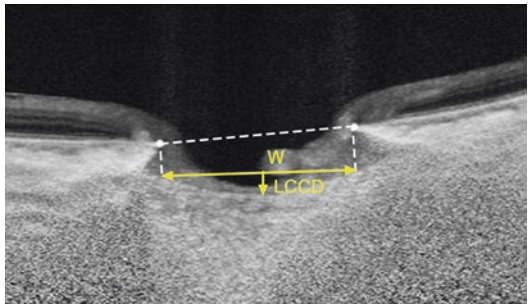

Fig. 5 Measurement of the lamina cribrosa curvature index (LCCI using a horizontal raster scan). The LC curvature depth (LCCD) was measured at the maximally depressed point as the distance from the reference line which connects two points at the anterior LC surface below the Bruch's membrane opening. The LCCI was measured by dividing the LC curve depth (LCCD) by the width of the reference line (W) and multiplying by 100. Adopted and modified from Lee et al. (2017)

named as LC curvature index (LCCI) (Lee et al. 2017). The LCCI was measured by measuring the LC depth from a reference line which was made by connecting two peripheral points on the anterior LC surface. The measured LC curve depth was divided by the width of the reference line and multiply by 100 (Fig. 5).

Another method that can be used in assessing the LC curve has been suggested by Kim et al. 2016a. They calculated the difference of mean mean depth from a reference line set in the LC surface and the LC insertion depth. To do this, they first measured the area demarcated by the reference line, two vertical lines from the LC insertion to the reference line, and the anterior LC surface. Then, the area was divided by the distance between the two LC insertions for the measurement of mean depth.

4.4 LC Insertion Depth

Posterior migration of the LC insertion has been recognized in histologic studies. Using a high quality LC images particularly with postprocessing by adaptive compensation, the LC insertion can be identified. The LC insertion depth can be measured from the anterior scleral opening level. Lee et al. (2014a) demonstrated that LC insertion depth was greater in eyes with POAG compared to healthy eyes, which accords to the histologic findings (Fig. 6). The utility of LC insertion depth in the clinical practice remains to be explored.

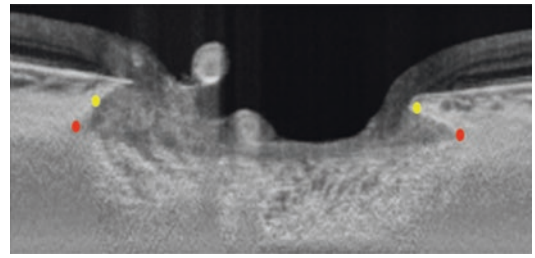

Fig. 6 LC insertion depth can be measured as the distance from the anterior scleral opening (yellow circles) to the LC insertion point (red circles)

5 Findings in Glaucoma

5.1 Thinner LC

LC thickness correlated significantly with visual field mean deviation (Inoue et al. 2009). Lee et al. (2011) demonstrated that LC thickness is smaller in eyes with glaucoma compared to healthy eyes.

Park et al. demonstrated that LC was thinner in the POAG and NTG groups than in the normal control group. Interestingly, they found that the lamina was also significantly thinner in patients with NTG and disc hemorrhage than in those with NTG but no disc hemorrhage (Park et al. 2012b).

A thinner LC would be associated with steeper translaminar pressure gradients when other conditions are equal (Jonas et al. 2004; Burgoyne et al. 2005). Therefore, it is not surprising that LC is thinner in eyes with glaucoma.

5.2 Dynamic Behavior According to IOP Change

Experimental glaucoma model studies demonstrated that LC morphology changes according to the variation of intraocular pressure. As it became possible to image the LC in patients, reduction of anterior LC depth and flattening of

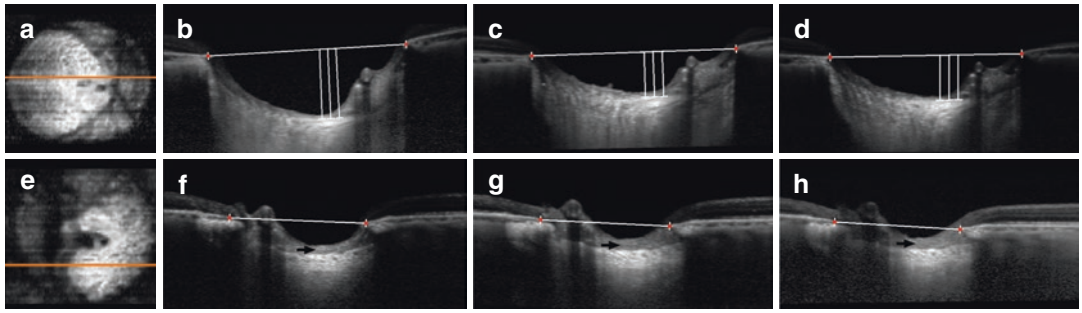

Fig. 7 Enface (**a**, **e**) and B-scan images obtained preoperatively (**b**, **f**) and at 1 (**c**, **g**) and 6 months (**d**, **h**) postoperatively in 15- (top) and 80-year-old (bottom) patients. Note the reduction of LC depth and LC curvature. The changes are seen more clearly in young patient. Adopted and modified from Lee et al. (2012)

the LC curve after IOP lowering treatment has been demonstrated (Fig. 7) (Lee et al. 2012, 2013b, 2016a, 2020; Barrancos et al. 2014; Krzyzanowska-Berkowska et al. 2018). Further, redisplacement of the anterior LC surface to the posterior direction has been demonstrated when the IOP re-elevated after bleb failure in patients who underwent trabeculectomy (Lee et al. 2013a). The anterior displacement of the anterior LC surface or flattening of the LC curve after IOP lowering is more prominent in young patients (Lee et al. 2012; Esfandiari et al. 2018), but also seen in elderly patients. The difference according to age suggests that the LC is more compliant and resilient according to IOP change in younger ages.

Theoretically, LC depth change can occur in opposite direction (i.e., posterior displacement upon IOP lowering). Finite element analysis has shown that anteroposterior displacement of the LC varied greatly depending on the properties of the lamina and sclera (Sigal et al. 2011). When the peripapillary sclera is more compliant than LC, IOP elevation can expand the canal, which in turn pulls the lamina taut from the sides. In this case, the LC depth may decrease when the IOP is increased. However, there has been little report which demonstrated this phenomenon in patients.

5.3 Greater LCCI

They demonstrated that LC curvature as assessed by LCCI also changes depending on the IOP change (Lee et al. 2016a). In addition, the LCCI performed better than LC depth measured from Bruch's membrane opening in discriminating between healthy and glaucomatous eyes (Lee et al. 2017). This finding suggests that the LC curvature may better characterize the glaucomatous LC deformation. This is probably because the LCCI is not affected by choroidal thickness. Kim et al. demonstrated that the LC curvature assessed by mean LC depth was greater in POAG eyes with high IOP than those with low IOP (Kim et al. 2016a).

The greater LCCI is associated with location of damage in individual patients. In unilateral glaucoma patients, glaucomatous eyes have greater LCCI than fellow healthy eyes (Kim et al. 2019b). Moreover, LCCI was greater in the hemifield corresponding with the location of RNFL defects compared to the opposite hemifield in glaucomatous eyes with hemifield optic nerve damage (Kim et al. 2019a).

5.4 Focal Lamina Defects

Several studies have demonstrated localized structural alteration of the peripheral LC, including focal LC defect and pit (Fig. 8). The focal LC defects were topographically correlated with localized neuroretinal rim loss, retinal nerve fiber layer defects, visual field defects, and parapapillary choroidal dropout (Park et al. 2013; You et al. 2013; Park et al. 2017a).

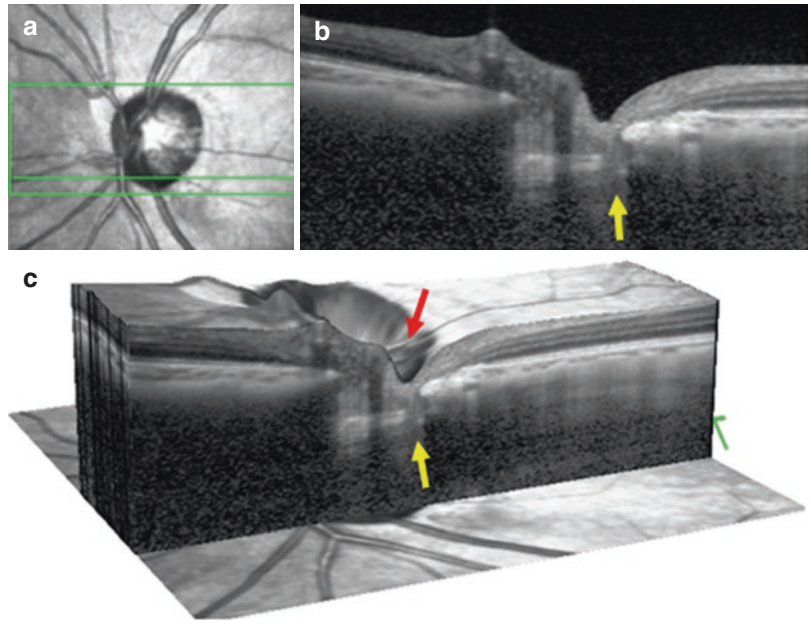

Fig. 8 Focal lamina cribrosa (LC) defect is seen in the B-scan (**b**) and reconstructed 3D images (**c**) at the location indicated in infrared photograph (green horizontal line in the inferior periphery, **a**) (yellow arrows). Focal neuroretinal rim is seen over the focal LC defect (red arrow)

5.5 Findings in Eyes with Disc Hemorrhage

Disc hemorrhage is often found in glaucoma patients and associated with glaucoma progression. The pathophysiology of disc hemorrhage is largely unveiled. Several LC imaging studies have suggested that LC deformation is associated with disc hemorrhage. Lee et al. demonstrated the structural alteration in the LC images obtained before and after DH, which were separated about 1 or 2 years (Fig. 9) (Lee et al. 2014b). This finding suggests that the DH may result from the disruption of capillaries in the laminar beams during the development of focal LC defect. In line with this finding, cross sectional studies demonstrated the association of DH and focal LC defects (Park et al. 2013; Kim and Park 2016; Kim et al. 2016b). Kim et al. have shown that the size of DH which corresponds to focal LC defect location tends to be larger than DH without correspondence (Kim et al. 2016b).

5.6 Association with Rate of Glaucoma Progression

Several characteristics of LC identified by OCT imaging have been found to be associated with rate of glaucoma progression. First, focal defects of the LC have been shown to be associated with the rate of glaucoma progression. Faridi et al. have shown that eyes with focal LC defects tend to progress faster than those without (Faridi et al. 2014). Park et al. demonstrated that glaucoma eyes with DH at the site of focal LC defects showed frequent and faster visual field progression compared with DH not accompanied by LC alterations or LC alterations not accompanied by DH (Park et al. 2017b). They reported in a separate article that the presence of focal LC defects was related to the rate of inferior RNFL thinning while a deeper and thinner LC was related to the rate of superior RNFL thinning (Park et al. 2017c).

Lee et al. investigated the relationship between LC change behavior and rate of glaucoma progression after trabeculectomy. They found that eyes with sustained LCD reduction over a long period had a slow rate of progressive RNFL thinning after trabeculectomy. A large LCD reduction in the early postoperative period was not associated with the long-term rate of progression if it was not maintained during subsequent follow-up (Lee and Kim 2015).

The LCCI has also been shown to be associated with the rate of visual field deterioration in POAG eyes (Ha et al. 2018). In addition, the

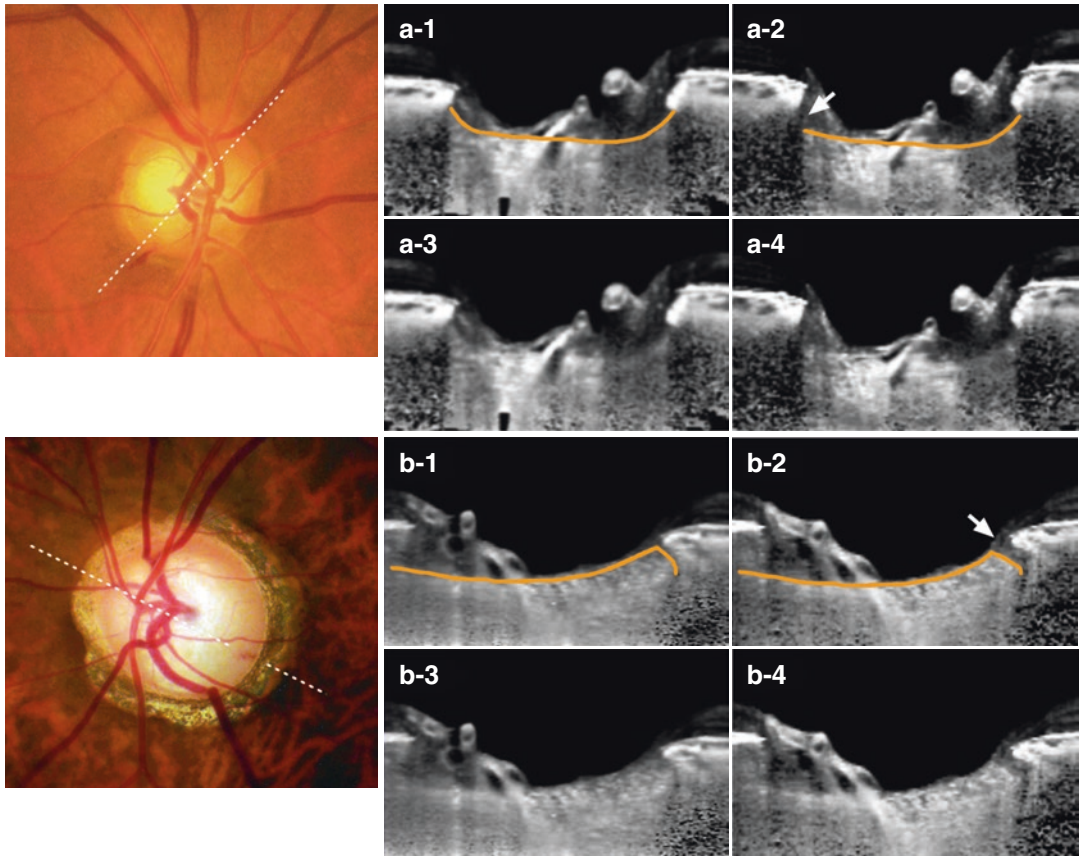

Fig. 9 Fundus photographs and SD-OCT B-scan images at the meridian (*dotted lines*) of disc hemorrhage. *Left images* (**a-1**, **a-3**, **b-1**, **b-3**) are the baseline B-scans and *right* (**a-2**, **a-4**, **b-2**, **b-4**) are the images obtained after detection of optic disc hemorrhage. *Orange lines* delineate the anterior surface of the lamina cribrosa (LC). (**a-3**, **a-4**) Same images as (**a-1**, **a-2**) without labels. (**b-3**, **b-4**) Same images as (**b-1**, **b-2**) without labels. (**a**) Structural alteration of the LC with outward deformation of the visible end of anterior LC surface. Note that the visible end of the anterior LC is more posteriorly located in the follow-up image (**a-2**, **b-2**) (*arrow*). The change in the curvature of the anterior LC surface also is noticeable (*orange lines*). (**b**) Recent structural alteration of the LC with radial disruption of the temporal LC. Note the enlarged cleft near the LC insertion in the follow-up image (*orange lines* and *arrow*). Adopted and modified from Lee et al. (2016b)

LCCI was associated with the rate of progressive RNFL thinning in glaucoma suspect eyes (Kim et al. 2018). This finding is consistent with experimental glaucoma model studies which demonstrated profoundly altered ONH connective tissues at the onset of detectable ONH surface change (Burgoyne et al. 2004). More recently, Lee et al. demonstrated that LCCI was the strongest prognostic factors for faster progressive RNFL thinning using regression tree model (Lee et al. 2019).

6 Applications of LC Imaging and Perspectives on Glaucoma Management

6.1 Differential Diagnosis from Other Optic Neuropathies

A characteristic feature of glaucoma is excavation of the optic nerve head (i.e., cupping). The excavation is composed of loss of neuronal tissue and posterior displacement/bowing of the lamina.

Mild degree of cupping is also noted in nonglaucomatous optic neuropathies, which often lead to misdiagnosis to glaucoma. Studies have shown that deep optic nerve head feature is different between glaucoma and other optic neuropathies. While deeply located or posteriorly curved LC together with loss of prelaminar tissue is the hallmark of glaucoma, those findings are not clearly seen in other optic neuropathies such as nonarteritic ischemic optic neuropathy and autosomal dominant optic neuropathy (Figs. 10 and 11) (Kim et al. 2020a; Fard et al. 2016; Lee et al. 2016b). This finding can be used to aid differential diagnosis in ambient cases with other differ-

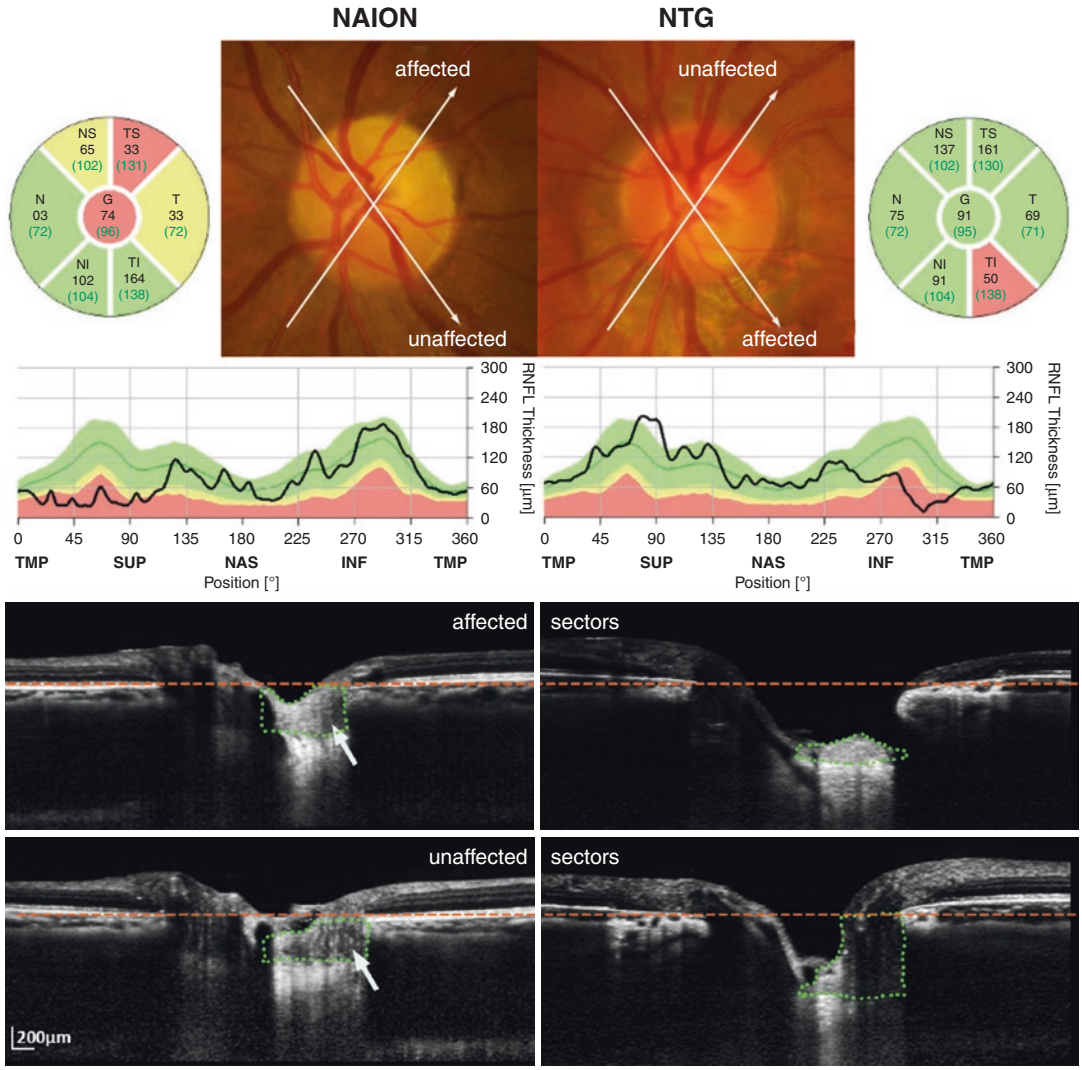

Fig. 10 Comparison of the prelaminar tissue thickness (PTT) between the affected and unaffected sectors in eyes with nonarteritic anterior ischemic optic neuropathy (NAION) (left) and normal tension glaucoma (NTG) (right). *Long arrows* in color disc photographs indicate the locations and directions of radial B-scans shown in the lower panels. *Orange dashed lines* indicate the level of the Bruch's membrane opening. *Green dotted lines* demarcate the area where the PTT was measured. Disc photographs in the top row show evident pallor (left) and notching (right) of the optic disc rims in the affected sectors in NAION and NTG eyes, respectively. Peripapillary OCT RNFL results show thinning of RNFL in the affected sectors in both NAION and NTG eyes. In NAION, the PT is thick in the affected sector, with the PTT being comparable to that in the unaffected sector (*arrows*). On the other hand, there is a remarkable difference in the PTT between the unaffected and the affected sectors in this NTG eye with an untreated IOP of 14 mmHg. Note that the anterior laminar surface is located deeper than in the affected sector than in the unaffected sector in NTG. Adopted and modified from Lee et al. (2016b)

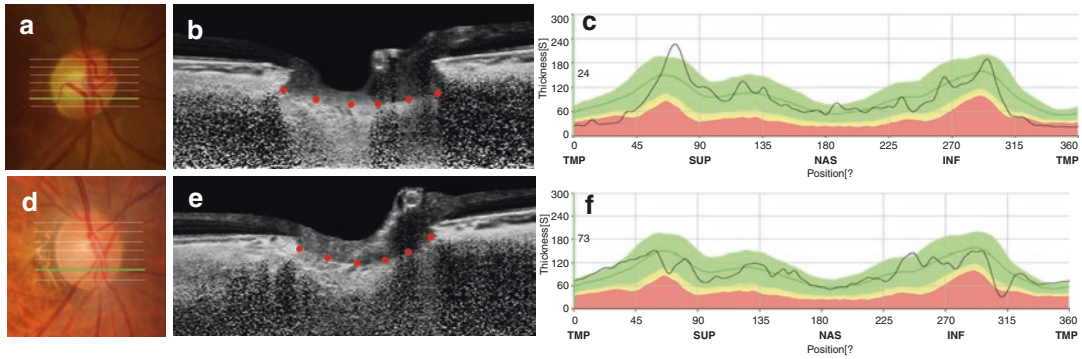

Fig. 11 Comparison of the anterior lamina cribrosa (red dots) curvature in an eye with autosomal dominant optic atrophy (ADOA) (**a**–**c**) in a 72-year-old woman, and an eye with normal tension glaucoma in a 77-year-old woman (**d**–**f**). (**b**, **e**) B-scan images at inferior midperipheral plane, indicated by the green lines in the optic disc photographs. (**c**) RNFL thinning is noted in the temporal region. (**f**) RNFL thinning is noted in the inferotemporal region. Adopted and modified from Kim et al. (2020b)

ential diagnosis point such more pronounced pallor than excavation, history of central vision loss and patter of visual field loss.

6.2 Predicting Rate of Future Glaucoma Progression

As describe earlier, several LC morphologic characteristics have been shown to be associated with rate of glaucoma progression as assessed by OCT or visual field in eyes with glaucoma. Those characteristics include thinner LC thickness, greater LCCI at baseline, presence of focal LC defects particularly with occurrence of disc hemorrhage (Ha et al. 2018; Faridi et al. 2014; Park et al. 2017b). The LC morphology can also be useful to predict development of glaucoma in suspect eyes (Fig. 12) (Kim et al. 2018). Characterization of high risk patients for disease progression will help clinicians to detect glaucoma progression early, so as to allow timely adjustment of the treatment.

6.3 Searching Mechanism of Optic Nerve Damage in Individual Patient

Glaucoma is a multifactorial disease. Although intraocular pressure induced stress is considered as the single most important risk factor, other factors including compromised circulation have been suggested as risk factors (Weinreb and Khaw 2004; Weinreb et al. 2014). Optic nerve damage often progresses despite substantial IOP lowering treatment. When a progression is noted despite maximum tolerable medical therapy, clinicians would consider other treatment options such as laser or surgical treatment for further IOP lowering. However, it is questionable whether such treatment approach is justified in every single glaucoma patient. This is due to the possibility that factors other than IOP related stress is the main cause of progression in certain patients.

There is no definite method to understand the mechanism of optic nerve damage in individual glaucoma patients. For better management of glaucoma, particularly for etiology targeted treatment approach, it is essential to develop method to identify specific etiology of optic nerve damage in individual patients. Theoretically, LC imaging can be a good candidate for such development because LC is a key structure in glaucoma biomechanics. The morphology of LC is variable among glaucoma patients, shedding light in this possibility. With further research and development of biomarkers, LC imaging might become a useful tool to help identify the specific mechanism of optic nerve damage in individual patients.

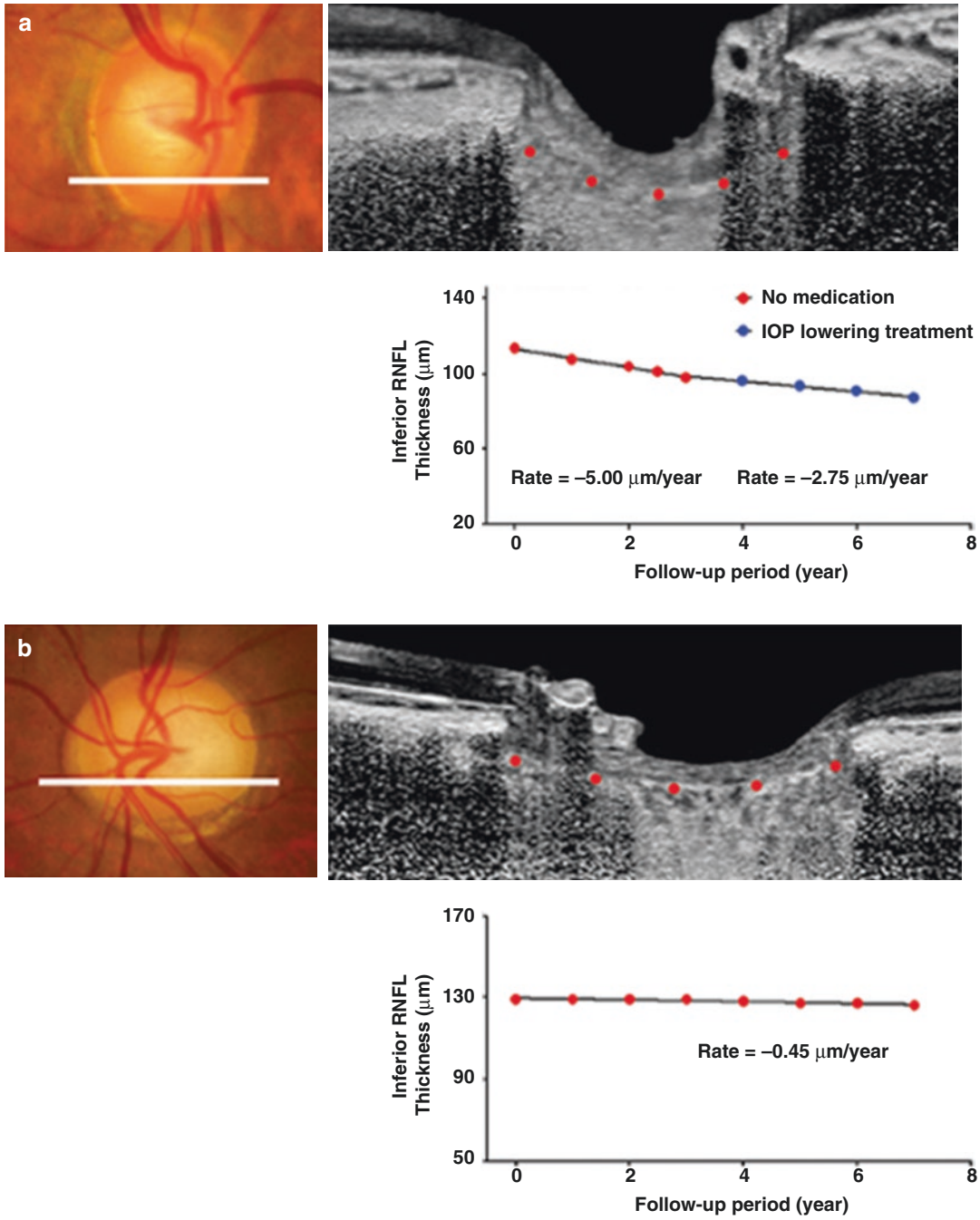

Fig. 12 Two cases of glaucoma suspect eyes. (**a**) A glaucoma suspect eye of a 61-year-old female with steeply curved lamina cribrosa (LC). The untreated intraocular pressure (IOP) and central corneal thickness were 16 mmHg and 537 μm, respectively. During the first 3 years following baseline examination, progressive retinal nerve fiber layer (RNFL) loss was observed in the inferior sector with the rate of −5.00 μm/year. After IOP lowering treatment, the rate of RNFL loss decreased to −2.75 μm/year. (**b**) A glaucoma-suspected eye of a 74-year-old female with a relatively fat LC. The untreated IOP and central corneal thickness were 16 mmHg and 545 μm, respectively. During 7 years of follow-up, the rate of RNFL loss in the inferior sector was −0.45 μm/year without any treatment. Adopted and modified from Kim et al. (2018)

6.4 Characterizing Optic Neuropathy in Myopic Eyes

Myopia is a risk factor for glaucoma (Mitchell et al. 1999; Liang et al. 2011; Suzuki et al. 2006). However, the rate of progression is often slower in myopic eyes with or even without IOP control (Lee et al. 2015; Araie et al. 2012). This finding suggests that mechanism of optic nerve damage may be different in myopic glaucomatous eyes. The LC configuration in myopic tilted disc eyes has some unique features. The LC is flatter and the pores are elongated to the direction of disc tilt/torsion (Fig. 13) (Sawada et al. 2018). This feature suggests that tensile stress to the LC arising from the axial elongation may play a role in the optic nerve damage.

If such stress is the main cause of optic nerve damage, the clinical course would be different from that of glaucoma derived from translaminar pressure gradient. Since axial elongation is not a lifelong process the tensile stress may be alleviated at some point. In addition, loss of axons may generate a room for remaining axons, thereby protecting them from the sustained tensile stress. If this is the case, the axonal loss can occur in the early life but the rate of loss can be slowed or halted in the late life (Kim et al. 2014). The treatment strategy should be different in those patients from the patients who have high risk of disease progression. Further study is needed to develop method to differentiate high risk and low risk patients for disease progression among myopic eyes. For those studies, LC imaging may play a central role.

7 Conclusions

Since LC is the primary site of axonal injury in glaucoma, imaging the LC provides an opportunity to enhance understanding on the pathogenesis of glaucomatous optic neuropathy. The LC imaging is not routinely used in the current clinical practice due to technical difficulty and lack of consensus in its utility. The devises for LC imaging and clinically useful biomarkers based on LC morphology are currently evolving. With further research and development, LC imaging may contribute to improvements in understanding biomechanics of glaucomatous optic neuropathy and specific mechanism of damage in individual patients, which will eventually facilitate development of patient-tailored treatment.

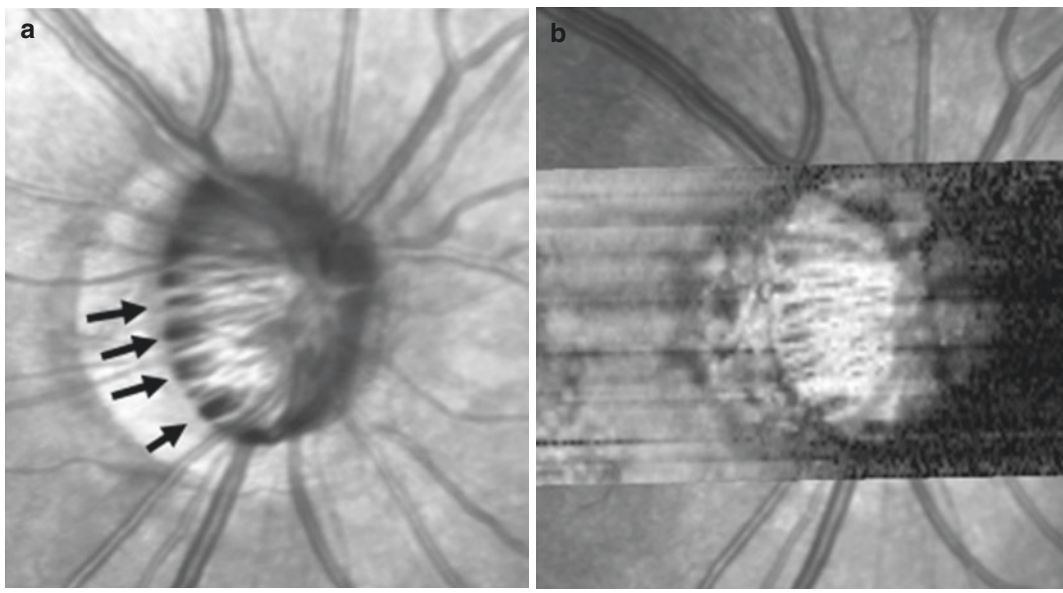

Fig. 13 Characteristic LC feature in myopic eyes shown in infrared fundus photo (**a**) and a coronal section of 3D reconstructed volume image (**b**). The laminar pores are large and elongated to the direction of disc tilt

References

Anderson DR, Hendrickson A. Effect of intraocular pressure on rapid axoplasmic transport in monkey optic nerve. Invest Ophthalmol. 1974;13(10):771–83.

Araie M, Shirato S, Yamazaki Y, Matsumoto C, Kitazawa Y, Ohashi Y, et al. Risk factors for progression of normal-tension glaucoma under beta-blocker monotherapy. Acta Ophthalmol. 2012;90(5):e337–43.

Barrancos C, Rebolleda G, Oblanca N, Cabarga C, Munoz-Negrete FJ. Changes in lamina cribrosa and prelaminar tissue after deep sclerectomy. Eye (Lond). 2014;28(1):58–65.

Burgoyne CF, Downs JC, Bellezza AJ, Hart RT. Three-dimensional reconstruction of normal and early glaucoma monkey optic nerve head connective tissues. Invest Ophthalmol Vis Sci. 2004;45(12):4388–99.

Burgoyne CF, Downs JC, Bellezza AJ, Suh JK, Hart RT. The optic nerve head as a biomechanical structure: a new paradigm for understanding the role of IOP-related stress and strain in the pathophysiology of glaucomatous optic nerve head damage. Prog Retin Eye Res. 2005;24(1):39–73.

Esfandiari H, Efatizadeh A, Hassanpour K, Doozandeh A, Yaseri M, Loewen NA. Factors associated with lamina cribrosa displacement after trabeculectomy measured by optical coherence tomography in advanced primary open-angle glaucoma. Graefes Arch Clin Exp Ophthalmol. 2018;256(12):2391–8.

Fard MA, Afzali M, Abdi P, Chen R, Yaseri M, Azaripour E, et al. Optic nerve head morphology in nonarteritic anterior ischemic optic neuropathy compared to open-angle glaucoma. Invest Ophthalmol Vis Sci. 2016;57(11):4632–40.

Faridi OS, Park SC, Kabadi R, Su D, De Moraes CG, Liebmann JM, et al. Effect of focal lamina cribrosa defect on glaucomatous visual field progression. Ophthalmology. 2014;121(8):1524–30.

Girard MJ, Tun TA, Husain R, Acharyya S, Haaland BA, Wei X, et al. Lamina cribrosa visibility using optical coherence tomography: comparison of devices and effects of image enhancement techniques. Invest Ophthal Vis Sci. 2015;56(2):865–74.

Goldbaum MH, Jeng SY, Logemann R, Weinreb RN. The extracellular matrix of the human optic nerve. Arch Ophthalmol. 1989;107(8):1225–31.

Ha A, Kim TJ, Girard MJA, Mari JM, Kim YK, Park KH, et al. Baseline lamina cribrosa curvature and subsequent visual field progression rate in primary open-angle glaucoma. Ophthalmology. 2018;125(12):1898–906.

Hernandez MR, Igoe F, Neufeld AH. Extracellular matrix of the human optic nerve head. Am J Ophthalmol. 1986;102(2):139–48.

Hernandez MR, Luo XX, Andrzejewska W, Neufeld AH. Age-related changes in the extracellular matrix of the human optic nerve head. Am J Ophthalmol. 1989;107(5):476–84.

Inoue R, Hangai M, Kotera Y, Nakanishi H, Mori S, Morishita S, et al. Three-dimensional high-speed optical coherence tomography imaging of lamina cribrosa in glaucoma. Ophthalmology. 2009;116(2):214–22.

Jonas JB, Berenshtein E, Holbach L. Lamina cribrosa thickness and spatial relationships between intraocular space and cerebrospinal fluid space in highly myopic eyes. Invest Ophthalmol Vis Sci. 2004;45(8):2660–5.

Kim YK, Park KH. Lamina cribrosa defects in eyes with glaucomatous disc haemorrhage. Acta Ophthalmol. 2016;94(6):e468–73.

Kim YW, Lee EJ, Kim TW, Kim M, Kim H. Microstructure of beta-zone parapapillary atrophy and rate of retinal nerve fiber layer thinning in primary open-angle glaucoma. Ophthalmology. 2014;121(7):1341–9.

Kim YW, Jeoung JW, Girard MJ, Mari JM, Park KH. Positional and curvature difference of lamina cribrosa according to the baseline intraocular pressure in primary open-angle glaucoma: a Swept-Source Optical Coherence Tomography (SS-OCT) study. PLoS One. 2016a;11(9):e0162182.

Kim YK, Jeoung JW, Park KH. Effect of focal lamina cribrosa defect on disc hemorrhage area in glaucoma. Invest Ophthalmol Vis Sci. 2016b;57(3):899–907.

Kim JA, Kim TW, Weinreb RN, Lee EJ, Girard MJA, Mari JM. Lamina cribrosa morphology predicts progressive retinal nerve fiber layer loss in eyes with suspected glaucoma. Sci Rep. 2018;8(1):738.

Kim JA, Kim TW, Lee EJ, Girard MJA, Mari JM. Lamina cribrosa morphology in glaucomatous eyes with hemifield defect in a Korean population. Ophthalmology. 2019a;126(5):692–701.

Kim JA, Kim TW, Lee EJ, Kim JM, Girard MJA, Mari JM. Intereye comparison of lamina cribrosa curvature in normal tension glaucoma patients with unilateral damage. Invest Ophthalmol Vis Sci. 2019b;60(7):2423–30.

Kim JA, Lee EJ, Kim TW, Kim H, Girard MJA, Mari JM, et al. Differentiation of nonarteritic anterior ischemic optic neuropathy from normal tension glaucoma by comparison of the lamina cribrosa. Invest Ophthalmol Vis Sci. 2020a;61(8):21.

Kim GN, Kim JA, Kim MJ, Lee EJ, Hwang JM, Kim TW. Comparison of lamina cribrosa morphology in normal tension glaucoma and autosomal-dominant optic atrophy. Invest Ophthalmol Vis Sci. 2020b;61(5):9.

Krzyzanowska-Berkowska P, Melinska A, Helemejko I, Robert Iskander D. Evaluating displacement of lamina cribrosa following glaucoma surgery. Graefes Arch Clin Exp Ophthalmol. 2018;256(4):791–800.

Lee EJ, Kim TW. Lamina cribrosa reversal after trabeculectomy and the rate of progressive retinal nerve fiber layer thinning. Ophthalmology. 2015;122(11):2234–42.

Lee EJ, Kim TW, Weinreb RN, Park KH, Kim SH, Kim DM. Visualization of the lamina cribrosa using enhanced depth imaging spectral-domain optical coherence tomography. Am J Ophthalmol. 2011;152(1):87–95. e1

Lee EJ, Kim TW, Weinreb RN. Reversal of lamina cribrosa displacement and thickness after trabeculectomy in glaucoma. Ophthalmology. 2012;119(7):1359–66.

Lee EJ, Kim TW, Weinreb RN. Variation of lamina cribrosa depth following trabeculectomy. Invest Ophthalmol Vis Sci. 2013a;54(8):5392–9.

Lee EJ, Kim TW, Weinreb RN, Kim H. Reversal of lamina cribrosa displacement after intraocular pressure reduction in open-angle glaucoma. Ophthalmology. 2013b;120(3):553–9.

Lee KM, Kim TW, Weinreb RN, Lee EJ, Girard MJ, Mari JM. Anterior lamina cribrosa insertion in primary open-angle glaucoma patients and healthy subjects. PLoS One. 2014a;9(12):e114935.

Lee EJ, Kim TW, Kim M, Girard MJ, Mari JM, Weinreb RN. Recent structural alteration of the peripheral lamina cribrosa near the location of disc hemorrhage in glaucoma. Invest Ophthalmol Vis Sci. 2014b;55(4):2805–15.

Lee JY, Sung KR, Han S, Na JH. Effect of myopia on the progression of primary open-angle glaucoma. Invest Ophthalmol Vis Sci. 2015;56(3):1775–81.

Lee SH, Yu DA, Kim TW, Lee EJ, Girard MJ, Mari JM. Reduction of the lamina cribrosa curvature after trabeculectomy in glaucoma. Invest Ophthalmol Vis Sci. 2016a;57(11):5006–14.

Lee EJ, Choi YJ, Kim TW, Hwang JM. Comparison of the deep optic nerve head structure between normal-tension glaucoma and nonarteritic anterior ischemic optic neuropathy. PLoS One. 2016b;11(4):e0150242.

Lee SH, Kim TW, Lee EJ, Girard MJ, Mari JM. Diagnostic power of lamina cribrosa depth and curvature in glaucoma. Invest Ophthalmol Vis Sci. 2017;58(2):755–62.

Lee EJ, Kim TW, Kim JA, Kim GN, Kim JM, Girard MJA, et al. Elucidation of the strongest factors influencing rapid retinal nerve fiber layer thinning in glaucoma. Invest Ophthalmol Vis Sci. 2019;60(10):3343–51.

Lee SH, Lee EJ, Kim JM, Girard MJA, Mari JM, Kim TW. Lamina cribrosa moves anteriorly after trabeculectomy in myopic eyes. Invest Ophthalmol Vis Sci. 2020;61(6):36.

Liang YB, Friedman DS, Zhou Q, Yang X, Sun LP, Guo LX, et al. Prevalence of primary open angle glaucoma in a rural adult Chinese population: the Handan eye study. Invest Ophthalmol Vis Sci. 2011;52(11):8250–7.

Mecham RP. Elastin synthesis and fiber assembly. Ann N Y Acad Sci. 1991;624:137–46.

Mitchell P, Hourihan F, Sandbach J, Wang JJ. The relationship between glaucoma and myopia: the Blue Mountains Eye Study. Ophthalmology. 1999;106(10):2010–5.

Morrison JC, L'Hernault NL, Jerdan JA, Quigley HA. Ultrastructural location of extracellular matrix components in the optic nerve head. Arch Ophthalmol. 1989;107(1):123–9.

Ogden TE, Duggan J, Danley K, Wilcox M, Minckler DS. Morphometry of nerve fiber bundle pores in the optic nerve head of the human. Exp Eye Res. 1988;46(4):559–68.

Park SC, Kiumehr S, Teng CC, Tello C, Liebmann JM, Ritch R. Horizontal central ridge of the lamina cribrosa and regional differences in laminar insertion in healthy subjects. Invest Ophthalmol Vis Sci. 2012a;53(3):1610–6.

Park HY, Jeon SH, Park CK. Enhanced depth imaging detects lamina cribrosa thickness differences in normal tension glaucoma and primary open-angle glaucoma. Ophthalmology. 2012b;119(1):10–20.

Park SC, Hsu AT, Su D, Simonson JL, Al-Jumayli M, Liu Y, et al. Factors associated with focal lamina cribrosa defects in glaucoma. Invest Ophthalmol Vis Sci. 2013;54(13):8401–7.

Park HY, Hwang YS, Park CK. Ocular characteristics associated with the location of focal lamina cribrosa defects in open-angle glaucoma patients. Eye (Lond). 2017a;31(4):578–87.

Park HL, Lee J, Jung Y, Park CK. Optic disc hemorrhage and lamina cribrosa defects in glaucoma progression. Sci Rep. 2017b;7(1):3489.

Park HL, Kim SI, Park CK. Influence of the lamina cribrosa on the rate of global and localized retinal nerve fiber layer thinning in open-angle glaucoma. Medicine (Baltimore). 2017c;96(14):e6295.

Quigley HA, Addicks EM. Regional differences in the structure of the lamina cribrosa and their relation to glaucomatous optic nerve damage. Arch Ophthalmol. 1981;99(1):137–43.

Quigley H, Anderson DR. The dynamics and location of axonal transport blockade by acute intraocular pressure elevation in primate optic nerve. Invest Ophthalmol. 1976;15(8):606–16.

Quigley HA, Hohman RM, Addicks EM, Massof RW, Green WR. Morphologic changes in the lamina cribrosa correlated with neural loss in open-angle glaucoma. Am J Ophthalmol. 1983;95(5):673–91.

Radius RL, Gonzales M. Anatomy of the lamina cribrosa in human eyes. Arch Ophthalmol. 1981;99(12):2159–62.

Rhodes LA, Huisingh C, Johnstone J, Fazio MA, Smith B, Wang L, et al. Peripapillary choroidal thickness variation with age and race in normal eyes. Invest Ophthalmol Vis Sci. 2015;56(3):1872–9.

Sawada Y, Araie M, Kasuga H, Ishikawa M, Iwata T, Murata K, et al. Focal lamina cribrosa defect in myopic eyes with nonprogressive glaucomatous visual field defect. Am J Ophthalmol. 2018;190:34–49.

Sigal IA, Yang H, Roberts MD, Grimm JL, Burgoyne CF, Demirel S, et al. IOP-induced lamina cribrosa deformation and scleral canal expansion: independent or related? Invest Ophthalmol Vis Sci. 2011;52(12):9023–32.

Suzuki Y, Iwase A, Araie M, Yamamoto T, Abe H, Shirato S, et al. Risk factors for open-angle glaucoma in a Japanese population: the Tajimi Study. Ophthalmology. 2006;113(9):1613–7.

Vianna JR, Lanoe VR, Quach J, Sharpe GP, Hutchison DM, Belliveau AC, et al. Serial changes in lamina cribrosa depth and neuroretinal parameters in glaucoma: impact of choroidal thickness. Ophthalmology. 2017;124(9):1392–402.

Weinreb RN, Khaw PT. Primary open-angle glaucoma. Lancet. 2004;363(9422):1711–20.

Weinreb RN, Aung T, Medeiros FA. The pathophysiology and treatment of glaucoma: a review. JAMA. 2014;311(18):1901–11.

You JY, Park SC, Su D, Teng CC, Liebmann JM, Ritch R. Focal lamina cribrosa defects associated with glaucomatous rim thinning and acquired pits. JAMA Ophthalmol. 2013;131(3):314–20.